Chapter 3

MATERIALS AND FABRICATION

3.1 Stator cores

Stator cores of AFPM brushless machines are made of laminated steels or soft magnetic powder materials. Soft magnetic powders simplify the manufacturing process and reduce the cost of AFPM machines.

3.1.1 Nonoriented electrical steels

Most laminated cores for stators of AFPM brushless machines are made of *nonoriented (isotropic) silicon steel* ribbons with standard thickness from 0.12 to 0.64 mm. Nonoriented steels are Fe-Si alloys with a random orientation of crystal cubes. Magnetic properties are practically the same in any direction in the plane of the sheet or ribbon. A secondary recrystallization process is not needed and high temperature annealing is not essential. Nonoriented grades contain between 0.5% and 3.25% Si with up to 0.5% Al addition to increase the resistivity and lower the temperature of the primary recrystallization.

Nonoriented electrical steels are available as both *fully processed* and *semi-processed* products. Fully processed nonoriented electrical steels are completely processed by the steel manufacturer, ready for use without any additional processing required to achieve the desired magnetic quality. Semi-processed nonoriented electrotechnical steels are those which have not been given the full annealing treatment by the steel producer. In some cases, users prefer to develop the final magnetic quality and achieve relief of fabricating stresses in laminations or assembled cores for small machines.

The most universally accepted grading of electrical steels by core losses is the American Iron and Steel Industry (AISI) system (Table 3.1), the so called "M-grading". For small and medium power electrical machines (output power

Table 3.1. The most important silicon steel designations specified by different standards

Europe IEC 404-8-4 (1986)	U.S.A. AISI	Japan JIS 2552 (1986)	Russia GOST 21427 0-75
250-35-A5	M-15	35A250	2413
270-35-A5	M-19	35A270	2412
300-35-A5	M-22	35A300	2411
330-35-A5	M-36	—	—
270-50-A5	—	50A270	—
290-50-A5	M-15	50A290	2413
310-50-A5	M-19	50A310	2412
330-50-A5	M-27	—	—
350-50-A5	M-36	50A350	2411
400-50-A5	M 43	50A400	2312
470-50-A5	—	50A470	2311
530-50-A5	M-45	—	2212
600-50-A5	—	50A600	2112
700-50-A5	M-47	50A700	—
800-50-A5	—	50A800	2111
350-65-A5	M-19	—	—
400-65-A5	M-27	—	—
470-65-A5	M-43	—	—
530-65-A5	—	—	2312
600-65-A5	M-45	—	2212
700-65-A5	—	—	2211
800-65-A5	—	65A800	2112
1000-65-A5	—	65A1000	—

less that 75 kW), the following grades can be used: M-27, M-36, M-43, M-45 and M-47.

Laminating a magnetic core is ineffective in keeping excessive eddy currents from circulating within the entire core unless the surfaces of laminations are adequately insulated. Types of surface insulation include the natural oxide surface, inorganic insulation, enamel, varnish or chemically treated surface. The thickness of the insulation is expressed with the aid of the *stacking factor*:

$$k_i = \frac{d}{d + 2\Delta} \tag{3.1}$$

where d is the thickness of bare lamination and Δ is the thickness of the insulation layer measured on one side. The stacking factor k_i is typically from 0.94 to 0.97.

Table 3.2. Specific core losses of *Armco* DI-MAX nonoriented electrical steels M-27, M-36 and M-43 at 60 Hz

Magnetic flux density T	Specific core losses W/kg							
	0.36 mm		0.47 mm			0.64 mm		
	M-27	M-36	M-27	M-36	M-43	M-27	M-36	M-43
0.20	0.09	0.10	0.10	0.11	0.11	0.12	0.12	0.13
0.50	0.47	0.52	0.53	0.56	0.59	0.62	0.64	0.66
0.70	0.81	0.89	0.92	0.97	1.03	1.11	1.14	1.17
1.00	1.46	1.61	1.67	1.75	1.87	2.06	2.12	2.19
1.30	2.39	2.58	2.67	2.80	2.99	3.34	3.46	3.56
1.50	3.37	3.57	3.68	3.86	4.09	4.56	4.70	4.83
1.60	4.00	4.19	4.30	4.52	4.72	5.34	5.48	5.60
1.70	4.55	4.74	4.85	5.08	5.33	5.99	6.15	6.28
1.80	4.95	5.14	5.23	5.48	5.79	6.52	6.68	6.84

Table 3.3. Magnetization curves of fully processed *Armco* DI-MAX nonoriented electrical steels M-27, M-36 and M-43

Magnetic flux density T	Magnetic field intensity A/m		
	M-27	M-36	M-43
0.20	36	41	47
0.40	50	57	64
0.70	74	80	89
1.00	116	119	130
1.20	175	174	187
1.50	859	785	777
1.60	2188	2109	1981
1.70	4759	4727	4592
1.80	8785	8722	8682
2.00	26 977	26 022	26 818
2.10	64 935	65 492	66 925
2.20	137 203	136 977	137 075

Core loss curves of *Armco* DI-MAX nonoriented electrical steels M-27, M-36 and M-43 tested at 60 Hz are given in Table 3.2. Core losses when tested at 50 Hz would be approximately 0.79 times the core loss at 60 Hz. Magnetization curves of the same electrical steels are given in Table 3.3. The specific

Table 3.4. Specific core losses and d.c. magnetization curve of nonoriented thin electrical steels manufactured by *Cogent Power Ltd.*, Newport, U.K.

Magn. flux dens. T	Specific core losses W/kg NO 12 0.12 mm 50 Hz	400 Hz	2.5 kHz	NO 18 0.18 mm 50 Hz	400 Hz	2.5 kHz	NO 20 0.2 mm 50 Hz	400 Hz	2.5 kHz	Magn. field stren. kA/m
0.10	0.02	0.16	1.65	0.02	0.18	2.18	0.02	0.17	2.79	0.025
0.20	0.08	0.71	6.83	0.08	0.73	10.6	0.07	0.72	10.6	0.032
0.30	0.16	1.55	15.2	0.16	1.50	19.1	0.14	1.49	24.4	0.039
0.40	0.26	2.57	2.54	0.26	2.54	31.7	0.23	2.50	40.4	0.044
0.50	0.37	3.75	37.7	0.36	3.86	45.9	0.32	3.80	58.4	0.051
0.60	0.48	5.05	52.0	0.47	5.22	61.5	042	5.17	78.4	0.057
0.70	0.62	6.49	66.1	0.61	6.77	81.1	0.54	6.70	103.0	0.064
0.80	0.76	8.09	83.1	0.75	8.47	104.0	0.66	8.36	133.0	0.073
0.90	0.32	9.84	103.0	0.90	10.4	161.0	0.80	10.3	205.0	0.084
1.00	1.09	11.8	156	1.07	12.3	198.0	0.95	12.2	253.0	0.099
1.10	1.31	14.1		1.28	14.9		1.14	14.8		0.124
1.20	1.56	16.7		1.52	18.1		1.36	17.9		0.160
1.30	1.89	19.9		1.84	21.6		1.65	21.4		0.248
1.40	2.29	24.0		2.23	25.6		2.00	25.3		0.470
1.50	2.74	28.5		2.67	30.0		2.40	29.7		1.290
1.60	3.14			3.06			2.75			3.550
1.70	3.49			3.40			3.06			7.070
1.80	3.78			3.69			3.32			13

mass density of DI-MAX M-27, M-36 and M-43 is 7650, 7700 and 7750 kg/m^3 respectively. The stacking factor is $k_i = 0.95$ to 0.96. The prefix DI-MAX, e.g. DI-MAX M27, designates a registered trademark with a special strip-annealed process that maximizes *punchability.* DI-MAX grades have superior permeability at high magnetic flux density, low core losses and good gauge uniformity. A smooth surface, excellent flatness and high stacking factor is obtained as a result of cold finishing and strip annealing.

For frequencies exceeding the power frequency of 50 or 60 Hz nonoriented laminations thinner than 0.2 mm must be used. Table 3.4 shows magnetization and specific core losses of nonoriented grades NO 12, NO 18 and NO 20 capable of operating up to 2.5 kHz (*Cogent Power Ltd.,* Newport, UK). Typical chemical composition is 3.0 % Si, 0.4 % Al, 96.6 % Fe. The standard thickness of an inorganic phosphate based insulation is 1 μm (one side). The maximum continuous operating temperature in the air is 230°C, maximum intermittent

Table 3.5. Physical properties of iron based METGLAS amorphous alloy ribbons (*Honeywell*, Morristown, NJ, U.S.A.)

Quantity	2605CO	2605SA1
Saturation magnetic flux density, T	1.8	1.59 annealed 1.57 cast
Specific core losses at 50 Hz and 1 T, W/kg	less than 0.28	about 0.125
Specific density, kg/m^3	7560	7200 annealed 7190 cast
Electric conductivity, S/m	0.813×10^6 S/m	0.769×10^6 S/m
Hardness in Vicker's scale	810	900
Elasticity modulus, GN/m^2	100...110	100...110
Stacking factor	less than 0.75	less than 0.79
Crystallization temperature, °C	430	507
Curie temperature, °C	415	392
Maximum service temperature, °C	125	150

operating temperature in an inert gas is 850°C, hardness 180 HV and density 7650 kg/m^3.

3.1.2 Amorphous ferromagnetic alloys

To minimize core losses at high frequencies, nonoriented electrotechnical steels should be replaced with *amorphous magnetic alloys* (Tables 3.5 and 3.6). Amorphous ferromagnetic alloys, in comparison with electrical steels with crystal structure, do not have arranged in order, regular inner crystal structure (lattice).

Amorphous alloy ribbons based on alloys of iron, nickel and cobalt are produced by rapid solidification of molten metals at cooling rates of about 10^6 °C/s. The alloys solidify before the atoms have a chance to segregate or crystal-

Table 3.6. Specific core losses of iron based METGLAS amorphous alloy ribbons (*Honeywell*, Morristown, NJ, U.S.A.)

Magnetic flux density, B T	Specific core losses, Δp, W/kg			
	2605CO		2605SA1	
	50 Hz	60 Hz	50 Hz	60 Hz
0.05	0.0024	0.003	0.0009	0.0012
0.10	0.0071	0.009	0.0027	0.0035
0.20	0.024	0.030	0.0063	0.008
0.40	0.063	0.080	0.016	0.02
0.60	0.125	0.16	0.032	0.04
0.80	0.196	0.25	0.063	0.08
1.00	0.274	0.35	0.125	0.16

lize. The result is a metal alloy with a glass-like structure, i.e. a non-crystalline frozen liquid.

Application of amorphous alloy ribbons to the mass production of electrical machines is limited by hardness, up to 1100 in Vicker's scale. Standard cutting methods like a guillotine or blank die are not suitable. The mechanically stressed amorphous material cracks. Laser and electro-discharge machining (EDM) cutting methods melt the amorphous material and cause undesirable crystallization. In addition, these methods make electrical contacts between laminations which contribute to the increased eddy-current and additional losses. In the early 1980s chemical methods were used in *General Electric* to cut amorphous materials but these methods were very slow and expensive [176]. The problem of cutting hard amorphous ribbons can be overcome by using a liquid jet [220]. This method makes it possible to cut amorphous materials in ambient temperature without cracking, melting, crystallization and electric contacts between isolated ribbons.

3.1.3 Soft magnetic powder composites

Powder metallurgy is used in the production of ferromagnetic cores of small electrical machines or ferromagnetic cores with complicated shapes. The components of *soft magnetic powder composites* are iron powder, dielectric (epoxy resin) and filler (glass or carbon fibers) for mechanical strengthening. Powder composites for ferromagnetic cores of electrical machines and apparatus can be divided into [236]:

- dielectromagnetics and magnetodielectrics,
- magnetic sinters.

Table 3.7. Magnetization and specific core loss characteristics of non-sintered *Accucore* (*TSC Ferrite International*, Wadsworth, IL, U.S.A.)

Magnetization curve		Specific core loss curves		
Magnetic flux density, B T	Magnetic field intensity, H A/m	60 Hz W/kg	100 Hz W/kg	400 Hz W/kg
0.10	152	0.132	0.242	1.058
0.20	233	0.419	0.683	3.263
0.30	312	0.772	1.323	6.217
0.40	400	1.212	2.072	9.811
0.50	498	1.742	2.976	14.088
0.60	613	2.315	3.968	18.850
0.70	749	2.954	5.071	24.295
0.80	909	3.660	6.305	30.490
0.90	1107	4.431	7.650	37.346
1.00	1357	5.247	9.039	44.489
1.10	1677	6.129	10.582	52.911
1.20	2101	7.033	12.214	61.377
1.30	2687	7.981	13.845	70.151
1.40	3525	8.929	15.565	79.168
1.50	4763	9.965	17.394	90.302
1.60	6563	10.869	19.048	99.671
1.70	9035	11.707	20.635	109.880
1.75	10,746	12.125	21.407	

Dielectromagnetics and magnetodielectrics are names referring to materials consisting of the same basic components: ferromagnetic (mostly iron powder) and dielectric (mostly epoxy resin) material [236]. The main tasks of the dielectric material is insulation and binding of ferromagnetic particles. In practice, composites containing up to 2% (of their mass) of dielectric materials are considered as *dielectromagnetics.* Those with a higher content of dielectric material are considered as *magnetodielectrics* [236].

TSC International, Wadsworth, IL, U.S.A., has developed a new soft powder material, *Accucore,* which is competitive to traditional steel laminations [4]. The magnetization curve and specific core loss curves of the non-sintered *Accucore* are given in Table 3.7. When sintered, *Accucore* has higher saturation magnetic flux density than the non-sintered material. The specific density is 7550 to 7700 kg/m^3.

Höganäs, Höganäs, Sweden, manufactures soft magnetic composite (SMC) powders that are surface-coated metal powders with excellent compressibility

Table 3.8. Specific core losses of Somaloy^{TM}500 +0.5% Kenolube, 800 MPa, treated at 500°C for 30 min in the air, *Höganäs*, Höganäs, Sweden

Magnetic flux density, A/m	Specific losses W/kg					
	50 Hz	100 Hz	300 Hz	500 Hz	700 Hz	1000 Hz
0.4	1.5	3	12	18	27	45
0.5	1.9	3.6	17	27	40	60
0.6	2.7	6	21	34	55	90
0.8	4.6	10	32	52	92	120
1.0	6.8	16	48	80	140	180
2.0	30	50	170	270	400	570

Table 3.9. Magnetization curves of Somaloy^{TM}500 +0.5% Kenolube, treated at 500°C for 30 min in the air, *Höganäs*, Höganäs, Sweden

Magnetic field intensity H A/m	B at density 6690 kg/m^3 T	B at density 7100 kg/m^3 T	B at density 7180 kg/m^3 T
1 500	0.7	0.83	0.87
3 200	0.8	1.13	1.19
4 000	0.91	1.22	1.28
6 000	1.01	1.32	1.38
10 000	1.12	1.42	1.51
15 000	1.24	1.52	1.61
20 000	1.32	1.59	1.69
40 000	1.52	1.78	1.87
60 000	1.65	1.89	1.97
80 000	1.75	1.97	2.05
100 000	1.82	2.02	2.10

[216]. *Somaloy^{TM}500* (Tables 3.8, 3.9) has been developed for 3D magnetic circuits of electrical machines, transformers, ignition systems and sensors.

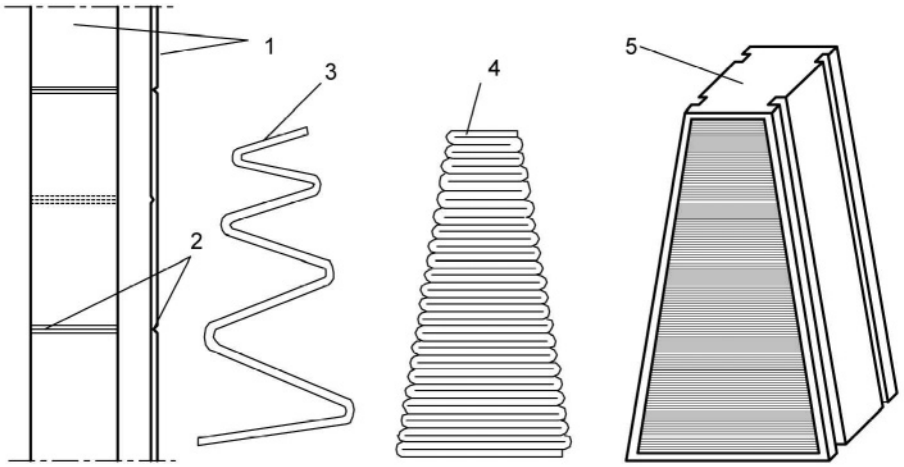

Figure 3.1. Stator core segment formed from lamination strip: 1 — lamination strip, 2 — groove, 3 — folding, 4 — compressed segment, 5 — finished segment.

3.1.4 Fabrication of stator cores

Fabrication of laminated stator cores

Normally, the stator cores are wound from electrotechnical steel strips and the slots are machined by shaping or planing. An alternative method is first to punch the slots with variable distances between them and then to wind the steel strip into the form of the slotted toroidal core (*R & D Institute of Electrical Machines VÚES* in Brno, Republic of Czech). In addition, this manufacturing process allows for making skewed slots to minimize the cogging torque and the effect of slot harmonics. Each stator core has skewed slots in opposite directions. It is recommended that a wave stator winding should be made to obtain shorter end connections and more space for the shaft. An odd number of slots, e.g. 25 instead of 24 can help to reduce the cogging torque (*VÚES* Brno).

Another technique is to form the stator core using trapezoidal segments [228]. Each segment corresponds to one slot pitch (Fig. 3.1). The lamination strip of constant width is folded at distances proportional to the radius. To make folding easy, the strip has transverse grooves on opposite sides of the alternative steps. The zigzag laminated segment is finally compressed and fixed using a tape or thermosetting, as shown in Fig. 3.1 [228].

Fabrication of soft magnetic powder stator cores

The laminated cores of axial flux machines are much more difficult to fabricate than those of radial flux machines. SMC powders simplify the manufacturing process of stator cores with complicated shapes, in general, 3D cores.

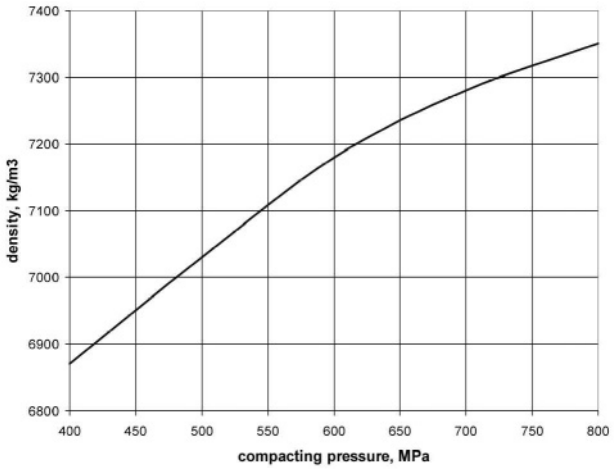

Figure 3.2. The effect of compacting pressure on the specific mass density of Höganäs soft magnetic composite powders.

Mass production of AFPM machines is much more cost effective if soft magnetic powder composites are used as materials for stator cores.

Using SMC powders the stator core of an AFPM machine can be made as a slotted core, slotless cylindrical core and salient pole core with one coil per pole.

The slotted and slotless cylindrical cores for AFPM machines can be made in a *powder metallurgy* process using a ferromagnetic powder with a small amount of lubricants or binders. The powder metallurgy process generally consists of four basic steps, namely: (1) powder manufacture, (2) mixing or blending, (3) compacting and (4) sintering. Most compacting is done with mechanical, hydraulic or pneumatic presses and rigid tools. Compacting pressures generally range between 70 to 800 MPa with 150 to 500 MPa being the most common. The outer diameter of the core is limited by the press capability. Frequently, the stator core must be divided into smaller segments. Most powder metallurgy products must have cross sections of less than 2000 mm^2. If the press capacity is sufficient, sections up to 6500 mm^2 can be pressed. Figure 3.2 shows the effect of compacting pressure on the density of *Höganäs* SMC powders.

For *Somaloy*^{TM} 500 the heat treatment temperature (sintering) is typically 500°C for 30 min. After heat treatment the compacted powder has much less mechanical strength than solid steel.

The thermal expansion of conductors within the stator slots creates thermal expansion stresses in the stator teeth. The magnitude of these stresses depends upon the difference in the temperature of the winding and core, difference in

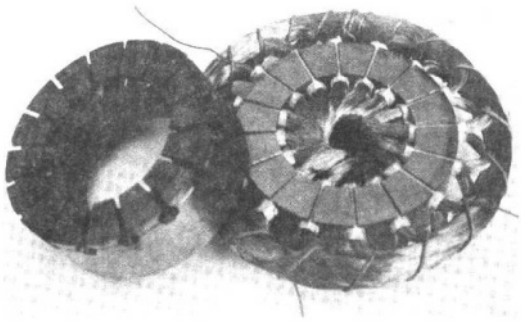

Figure 3.3. Slotted stators for small single-sided disc-type motors [236].

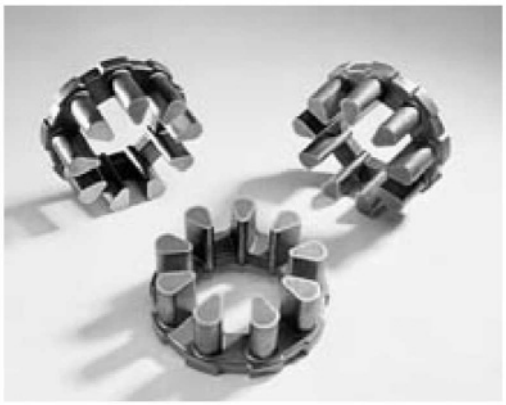

Figure 3.4. Powder salient pole stators for small single-sided AFPM motors. Courtesy of *Mii Technologies, LLC,* West Lebanon, NH, U.S.A.

coefficients of thermal expansion of both materials and slot fill factor. This problem is more important in powder cores than in laminated cores since the tensile stress of powder cores is at least 25 times lower and their modulus of elasticity is less than 100 GPa (versus 200 GPa for steel laminations).

Slotted stators for small disc-type motors fabricated from SMC powders are shown in Fig. 3.3 [148, 236]. SMC powder salient-pole stators for small single-sided AFPM motors manufactured by *Mii Technologies, LLC,* Lebanon, NH, U.S.A. are shown in Fig. 3.4. The three-phase stator has 9 poles. A single SMC powder salient pole manufactured by *Höganäs* is shown in Fig. 3.5.

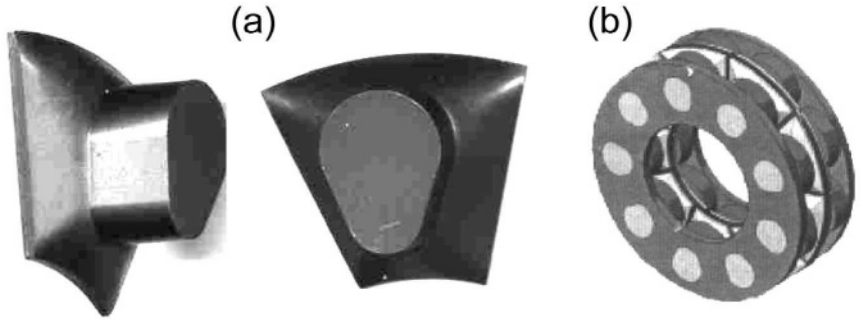

Figure 3.5. SMC powder salient pole for small single-sided AFPM motors: (a) single SMC pole; (b) double-sided AFPM motor. Courtesy of *Höganäs,* Höganäs, Sweden.

3.2 Rotor magnetic circuits

Magnetic circuits of rotors consist of PMs and mild steel backing rings or discs. Since the air gap is somewhat larger that that in similar RFPM counterparts, high energy density PMs should be used.

Normally, surface magnets are glued to smooth backing rings or rings with cavities of the same shape as magnets without any additional mechanical protection against normal attractive forces. Epoxy, acrylic or silicon based adhesives are used for gluing between magnets and backing rings or between magnets. The minimum required shearing strength of adhesives is 20×10^6 Pa. There were attempts to develop interior PM rotor for AFPM machines. According to [201], rotor poles can only be fabricated by using soft magnetic powders [201]. The main advantage of this configuration is the improved flux weakening performance. However, the complexity and high cost of the rotor structure discourage further commercializing development.

3.2.1 PM materials

A PM can produce magnetic flux in an air gap with no exciting winding and no dissipation of electric power. As any other ferromagnetic material, a PM can be described by its B—H hysteresis loop. PMs are also called *hard magnetic materials,* which means ferromagnetic materials with a wide hysteresis loop.

The basis for the evaluation of a PM is the portion of its hysteresis loop located in the upper left-hand quadrant, called the *demagnetization curve* (Fig. 3.6). If reverse magnetic field intensity is applied to a previously magnetized, say, toroidal specimen, the magnetic flux density drops down to the magnitude determined by the point *K.* When the reversal magnetic flux density is removed, the flux density returns to the point *L* according to a minor hysteresis loop. Thus, the application of a reverse field has reduced the *remanence,* or

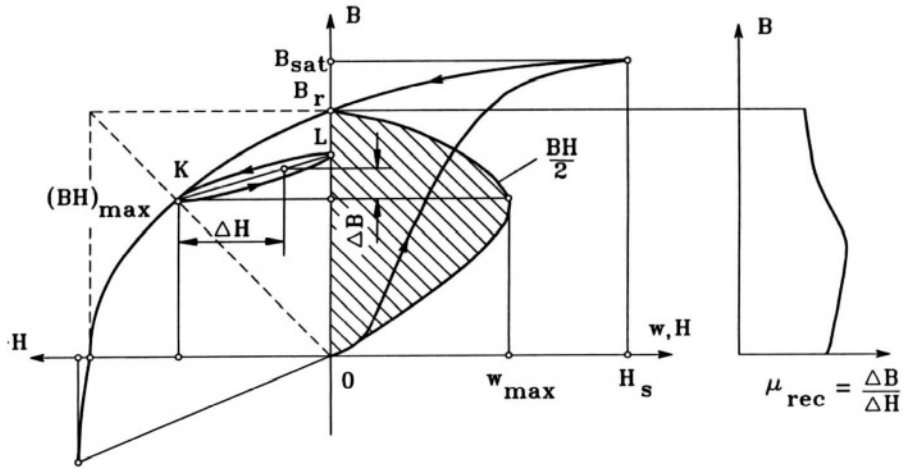

Figure 3.6. Demagnetization curve, recoil loop, energy of a PM, and recoil magnetic permeability.

remanent magnetism. Reapplying magnetic field intensity will again reduce the flux density, completing the minor hysteresis loop by returning the core to approximately the same value of flux density at the point *K* as before. The minor hysteresis loop may usually be replaced with little error by a straight line called the *recoil line.* This line has a slope called the *recoil permeability* μ_{rec}.

As long as the negative value of applied magnetic field intensity does not exceed the maximum value corresponding to the point *K,* the PM may be regarded as being reasonably permanent. If, however, greater negative field intensity *H* is applied, the magnetic flux density will be reduced to a value lower than that at point *K.* On the removal of *H,* a new and lower recoil line will be established.

Remanent magnetic flux density B_r, or *remanence,* is the magnetic flux density corresponding to zero magnetic field intensity.

Coercive field strength H_c, or *coercivity,* is the value of demagnetizing field intensity necessary to bring the magnetic flux density to zero in a material previously magnetized.

Both B_r and H_c decrease as the magnet temperature increases, i.e.

$$B_r = B_{r20}[1 + \frac{\alpha_B}{100}(\vartheta_{PM} - 20)] \tag{3.2}$$

$$H_c = H_{c20}[1 + \frac{\alpha_H}{100}(\vartheta_{PM} - 20)] \tag{3.3}$$

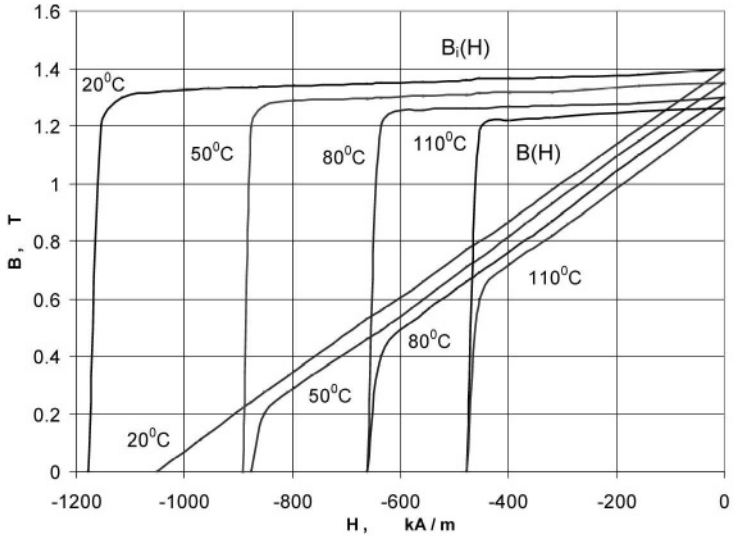

Figure 3.7. Comparison of *B—H* and B_i—H demagnetization curves and their variations with the temperature for sintered N48M NdFeB PMs. Courtesy of *ShinEtsu,* Takefu-shi, Fukui Prefecture, Japan.

where ϑ_{PM} is the temperature of PM, B_{r20} and H_{c20} are the remanent magnetic flux density and coercive force at 20°C and $\alpha_B < 0$ and $\alpha_H < 0$ are *temperature coefficients* for B_r and H_c in %/°C respectively. Thus, demagnetization curves are sensitive to the temperature (Fig. 3.7).

Intrinsic demagnetization curve (Fig. 3.7) is the portion of the $B_i = f(H)$ hysteresis loop located in the upper left-hand quadrant, where $B_i = B - \mu_0 H$. For $H = 0$ the intrinsic magnetic flux density $B_i = B_r$.

Intrinsic coercivity ${}_iH_c$ is the magnetic field strength required to bring to zero the intrinsic magnetic flux density B_i of a magnetic material described by the $B_i = f(H)$ curve. For PM materials ${}_iH_c > H_c$.

Saturation magnetic flux density B_{sat} corresponds to high values of the magnetic field intensity, when an increase in the applied magnetic field produces no further effect on the magnetic flux density. In the *saturation region* the alignment of all the *magnetic moments of domains* is in the direction of the external applied magnetic field.

Recoil magnetic permeability μ_{rec} is the ratio of the magnetic flux density–to–magnetic field intensity at any point on the demagnetization curve, i.e.

$$\mu_{rec} = \mu_o \mu_{rrec} = \frac{\Delta B}{\Delta H} \tag{3.4}$$

where the *relative recoil permeability* $\mu_{rrec} = 1 \ldots 4.5$.

Maximum magnetic energy per unit produced by a PM in the external space is equal to the maximum magnetic energy density per volume, i.e.

$$w_{max} = \frac{(BH)_{max}}{2} \qquad \mathrm{J/m^3} \tag{3.5}$$

where the product $(BH)_{max}$ corresponds to the maximum energy density point on the demagnetization curve with coordinates B_{max} and H_{max} (Fig. 3.6).

Form factor of the demagnetization curve characterizes the concave shape of the demagnetization curve, i.e.

$$\gamma = \frac{(BH)_{max}}{B_r H_c} = \frac{B_{max} H_{max}}{B_r H_c} \tag{3.6}$$

for a square demagnetization curve $\gamma = 1$ and for a straight line (rare-earth PMs) $\gamma = 0.25$.

The leakage flux causes the magnetic flux to be distributed nonuniformly along the height $2h_M$ of a PM, where h_M is the height per pole. As a result, the MMF produced by the PM is not constant. The magnetic flux is higher in the neutral cross section and lower at the ends, but the behavior of the MMF distribution is the opposite [96].

The PM surface is not equipotential. The magnetic potential at each point on the surface is a function of the distance to the neutral zone. To simplify the calculation, the magnetic flux which is a function of the MMF distribution along the height h_M per pole is replaced by an equivalent flux. This equivalent flux goes through the whole height h_M and exits from the surface of the poles. To find the equivalent leakage flux and the whole flux of a PM, the equivalent magnetic field intensity needs to be found, i.e.

$$H = \frac{1}{h_M} \int_0^{h_M} H_x dx = \frac{\mathcal{F}_M}{h_M} \tag{3.7}$$

where H_x is the magnetic field intensity at a distance x from the neutral cross section and $\mathcal{F}_M$ is the MMF of the PM per pole (MMF $- 2\mathcal{F}_M$ per pole pair).

The equivalent magnetic field intensity (3.7) allows the equivalent leakage flux of the PM to be found, i.e.

$$\Phi_{lM} = \Phi_M - \Phi_g \tag{3.8}$$

where Φ_M is the full equivalent flux of the PM and Φ_g is the air gap magnetic flux. The *coefficient of leakage flux* of the PM,

$$\sigma_{lM} = \frac{\Phi_M}{\Phi_g} = 1 + \frac{\Phi_{lM}}{\Phi_g} > 1 \tag{3.9}$$

simply allows the air gap magnetic flux to be expressed as $\Phi_g = \Phi_M/\sigma_{lM}$.

The following leakage permeance expressed in the flux Φ–MMF coordinate system corresponds to the equivalent leakage flux of the PM:

$$G_{lM} = \frac{\Phi_{lM}}{\mathcal{F}_M} \tag{3.10}$$

An accurate estimation of the leakage permeance G_{lM} is the most difficult task in analytical calculation of magnetic circuits with PMs. Using the field approach, e.g. the FEM, the leakage permeance can be found fairly accurately.

The average equivalent magnetic flux and equivalent MMF mean that the magnetic flux density and magnetic field intensity are assumed to be the same in the whole volume of a PM. The full energy produced by the magnet in the outer space is

$$W = \frac{BH}{2} V_M \qquad \text{J} \tag{3.11}$$

where V_M is the volume of the PM or a system of PMs.

For a PM circuit with a rectangular cross section, single PM and two mild steel pole shoes, the magnetic flux density B_g in a given air gap volume $V_g = gw_M l_M$ is directly proportional to the square root of the magnetic energy product $(B_M H_M)$ [96], i.e.

$$\begin{aligned} B_g = \mu_0 H_g &= \sqrt{\frac{\mu_0}{\sigma_{lM}} \left(1 + \frac{2H_{Fe} l_{Fe}}{H_g g}\right)^{-1} \frac{V_M}{V_g} B_M H_M} \\ &\approx \sqrt{\mu_o \frac{V_M}{V_g} B_M H_M} \end{aligned} \tag{3.12}$$

where H_{Fe} is the magnetic field intensity in the mild steel yoke, H_g is the magnetic field intensity in the air gap, $V_M = 2h_M w_M l_M$ is the magnet volume, w_M is the PM width, l_M is the PM length and $2l_{Fe}$ is the length of the magnetic flux path in two mild steel pole shoes. Following the trend to smaller packaging, smaller mass and higher efficiency, the material research in the field of PMs has focused on finding materials with high values of the maximum energy product $(BH)_{max}$.

The air gap magnetic flux density B_g can be estimated analytically on the basis of the demagnetization curve, air gap and leakage permeance lines and

recoil lines [96]. Approximately, it can be found on the basis of the balance of the magnetic voltage drops, i.e.

$$\frac{B_r}{\mu_0 \mu_{rrec}} h_M = \frac{B_g}{\mu_0 \mu_{rrec}} h_M + \frac{B_g}{\mu_0} g$$

where μ_{rrec} is the relative permeability of the PM (relative recoil permeability). Hence,

$$B_g \approx \frac{B_r h_M}{h_M + \mu_{rrec} g} = \frac{B_r}{1 + \mu_{rrec} g / h_M} \tag{3.13}$$

The air gap magnetic flux density is proportional to the remanent magnetic flux density B_r and decreases as the air gap g increases. Eqn (3.13) can only be used for preliminary calculations.

For rare-earth PMs the approximation of the demagnetization curve is simple due to practically linear demagnetization curve, i.e.

$$B(H) = B_r \left(1 - \frac{H}{H_c}\right) \tag{3.14}$$

The approximation of more complicated demagnetizations curves (Alnico or ferrites) is given e.g. in [96].

The intersection point of the above demagnetization curve (3.14) and the following line representing the permeance of the air gap

$$B(H) = \mu_0 \frac{h_M}{g} H \tag{3.15}$$

gives a point called the *operating point.* This point corresponds to the air gap magnetic flux density B_g multiplied by the leakage coefficient σ_{lM} according to eqn (3.9).

3.2.2 Characteristics of PM materials

There are three classes of PMs currently used for electric motors:

- Alnicos (Al, Ni, Co, Fe);
- Ceramics (ferrites), e.g. barium ferrite $BaO \times 6Fe_2O_3$ and strontium ferrite $SrO \times 6Fe_2O_3$;
- Rare-earth materials, i.e. samarium-cobalt SmCo and neodymium-iron-boron NdFeB.

The demagnetization curves of the above three types of permanent magnet materials are given in Fig. 3.8.

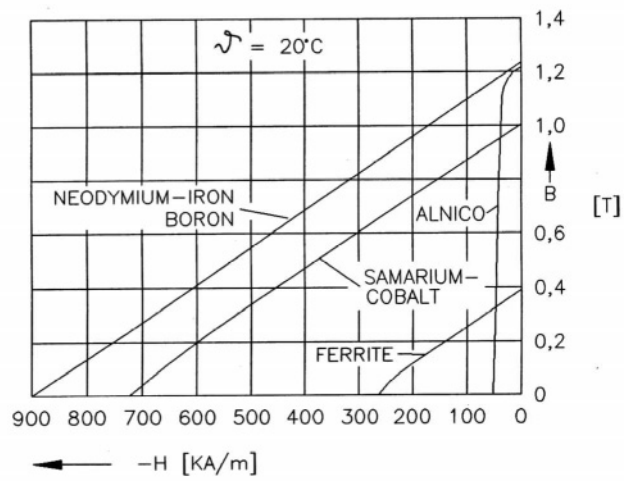

Figure 3.8. Demagnetization curves for different PM materials.

Alnico

Alnico magnets dominated the PM motor market in the range from a few watts to 150 kW between the mid 1940s and the late 1960s. The main advantages of Alnico are its high magnetic remanent flux density and low temperature coefficients (Table 3.10). The temperature coefficient of B_r is $-0.02\%/°\text{C}$ and maximum service temperature is 520°C. Unfortunately, the coercive force is very low and the demagnetization curve is extremely non-linear. Therefore, it is very easy not only to magnetize but also to demagnetize Alnico. Alnico has been used in PM d.c. commutator motors of the disc type with relatively large air gaps. This results in a negligible armature reaction magnetic flux acting on the PMs. Sometimes, Alnico PMs are protected from the armature flux, and consequently from demagnetization, using additional mild steel pole shoes.

Ferrites

Barium and strontium *ferrites* produced by powder metallurgy were invented in the 1950s. Their chemical formulation may be expressed as $\text{MO} \times 6(\text{Fe}_2\text{O}_3)$, where M is Ba, Sr, or Pb. Ferrite magnets are available in *isotropic* and *anisotropic* grades.

A ferrite has a higher coercive force than Alnico, but at the same time has a lower remanent magnetic flux density (Table 3.10). Temperature coefficients are relatively high, i.e. the coefficient of B_r is $-0.20\%/°\text{C}$ and the coefficient of H_c is -0.27 to $-0.4\%/°\text{C}$. The maximum service temperature is 450°C. The main advantages of ferrites are their low cost and very high electric re-

Table 3.10. Physical properties of a representative selection of PM materials for small motors offered by *Magnaquench GmBH*, Essen, Germany

Property	Alnico sintered Koerzit 500	Hard ferrite bonded Koerox 12/22p	Hard ferrite sintered Koerox 350
Remanent flux density, B_r, T	1.24	0.26	0.39
Coercivity, H_c, kA/m	51	180	270
Intrinsic coercivity, iH_c, kA/m	51	225	310
$(BH)_{max}$, kJ/m^3	41.4	13	30
Relative recoil magnetic permeability	3 to 4.5	1.1	1.1
Temperature coefficient α_B of B_r at 20 to 100°C, %/°C	−0.02	−0.2	−0.2
Temperature coefficient α_{iH} of iH_c at 20 to 100°C, %/°C	+0.03 to −0.07	+0.4	+0.3
Curie temperature, °C	850	450	450
Maximum continuous service temperature, °C	500	100 to 200	200
Thermal conductivity, W/(m °C)	10 to 100	–	4
Specific mass density, ρ_{PM}, kg/m^3	7300	3400	4800
Electric conductivity, S/m	1.4 to 2.5 $\times 10^6$	< 0.0001	< 0.0001
Coefficient of thermal expansion at 20 to 100°C, $\times 10^{-6}$/°C	11 to 13	20 to 50	12 parallel 8 vertical
Specific heat, J °C/kg	350 to 500	–	800

sistance, which means practically no eddy-current losses in the PM volume. Ferrite magnets are most economical in fractional horsepower motors. Barium ferrite PMs are commonly used in small d.c. commutator motors for automobiles (blowers, fans, windscreen wipers, pumps, etc.) and electric toys.

Rare-earth permanent magnets

The first generation of *rare-earth permanent magnets,* i.e. alloys based on the composition of $SmCo_5$ has been commercially produced since the early 1970s (invented in the 1960s). $SmCo_5$ has the advantage of a high remanent flux density, high coercive force, high energy product, a linear demagnetization curve and a low temperature coefficient (Table 3.11). The temperature coefficient of B_r is – 0.02 to – 0.045%/°C and the temperature coefficient of II_c is −0.14 to −0.40%/°C. Maximum service temperature is 300 to 350°C. It is suitable for motors with low volumes and motors operating at increased temperatures, e.g. brushless generators for microturbines. Both Sm and Co are relatively expensive due to their supply restrictions.

Table 3.11. Physical properties of Vacomax sintered Sm_2Co_{17} PM materials at room temperature 20°C manufactured by *Vacuumschmelze GmbH*, Hanau, Germany

Property	Vacomax 240 HR	Vacomax 225 HR	Vacomax 240
Remanent flux density, B_r, T	1.05 to 1.12	1.03 to 1.10	0.98 to 1.05
Coercivity, II_c, kA/m	600 to 730	720 to 820	580 to 720
Intrinsic coercivity, iH_c, kA/m	640 to 800	1590 to 2070	640 to 800
$(BH)_{max}$, kJ/m^3	200 to 240	190 to 225	180 to 210
Relative recoil magnetic permeability	1.22 to 1.39	1.06 to 1.34	1.16 to 1.34
Temperature coefficient α_B of B_r at 20 to 100°C, %/°C		−0.030	
Temperature coefficient α_{iH} of iH_c at 20 to 100°C, %/°C	−0.15	−0.18	−0.15
Temperature coefficient α_B of B_r at 20 to 150°C, %/°C		−0.035	
Temperature coefficient α_{iH} of iH_c at 20 to 150°C, %/°C	−0.16	−0.19	−0.16
Curie temperature, °C		approximately 800	
Maximum continuous service temperature, °C	300	350	300
Thermal conductivity, W/(m °C)		approximately 12	
Specific mass density, ρ_{PM}, kg/m^3		8400	
Electric conductivity, $\times 10^6$ S/m		1.18 to 1.33	
Coefficient of thermal expansion at 20 to 100°C, $\times 10^{-6}$/°C		10	
Young's modulus, $\times 10^6$ MPa		0.150	
Bending stress, MPa		90 to 150	
Vicker's hardness		approximately 640	

With the discovery in the recent years of a second generation of rare-earth magnets on the basis of inexpensive neodymium (Nd), remarkable progress with regard to lowering raw material costs has been achieved. The new generation of rare-earth PMs based on inexpensive neodymium (Nd) was announced by *Sumitomo Special Metals,* Japan, in 1983 at the 29th Annual Conference of Magnetism and Magnetic Materials held in Pittsburgh, PA, U.S.A. The Nd is a much more abundant rare-earth element than Sm. NdFeB magnets, which are now produced in increasing quantities have better magnetic properties (Table 3.12) than those of SmCo, but unfortunately only at room temperature. The demagnetization curves, especially the coercive force, are strongly temperature dependent. The temperature coefficient of B_r is – 0.09 to – 0.15%/°C and the temperature coefficient of H_c is – 0.40 to – 0.80%/°C. The maximum service

temperature is 250°C and Curie temperature is 350°C. The NdFeB is also susceptible to corrosion. NdFeB magnets have great potential for considerably improving the *performance–to–cost* ratio for many applications. For this reason they will have a major impact on the development and application of PM machines in the future.

Chemical reactivity of rare-earth magnets is similar to that of alkaline earth metals, e.g. magnesium. The reaction is accelerated at increased temperature and humidity. The NdFeB alloy if exposed to hydrogen gas, usually at a slightly elevated temperature and/or elevated pressure, becomes brittle and with very little effort, it can be crushed. Diffusion of hydrogen into the alloy causes it literally to fall apart.

Corrosion protective coatings can be divided into metallic and organic. For metallic coatings, e.g. nickel and tin, galvanic processes are used as a rule. Organic coatings include powder coatings applied electrostatically, varnishes and resins.

Nowadays, for the industrial production of rare-earth PMs the powder metallurgical route is mainly used [194]. Apart from some material specific parameters, this processing technology is, in general, the same for all rare-earth magnet materials. The alloys are produced by vacuum induction melting or by a calciothermic reduction of the oxides. The material is then size-reduced by crushing and milling to a single crystalline powder with particle sizes less than 10 μm. In order to obtain anisotropic PMs with the highest possible $(BH)_{max}$ value, the powders are then aligned in an external magnetic field, pressed and densified to nearly theoretical density by sintering. The most economical method for mass production of simply shaped parts like blocks, rings or arc segments is die pressing of the powders in approximately the final shape.

Researchers at *General Motors,* U.S.A., developed a fabrication method based on the melt-spinning casting system originally invented for the production of amorphous metal alloys. In this technology a molten stream of NdFeCoB material is first formed into ribbons 30 to 50-μm thick by rapid quenching, then cold pressed, extruded and hot pressed into bulk. Hot pressing and hot working are carried out while maintaining the fine grain to provide a high density close to 100% which eliminates the possibility of internal corrosion. The standard electro-deposited epoxy resin coating provides excellent corrosion resistance.

The prices of NdFeB magnets ordered in large quantities are now below US$20 per kg. Owing to a large supply of NdFeB magnets from China it is expected that the prices will fall further.

3.2.3 Operating diagram

The energy of a PM in the external space only exists if the reluctance of the external magnetic circuit is higher than zero. If a previously magnetized PM

Table 3.12. Physical properties of Hicorex-Super sintered NdFeB PM materials at room temperature 20°C manufactured by *Hitachi Metals, Ltd.*, Tokyo, Japan

Property	Hicorex-Super HS-38AV	Hicorex-Super HS-25EV	Hicorex-Super HS-47AH
Remanent flux density, B_r, T	1.20 to 1.30	0.98 to 1.08	1.35 to 1.43
Coercivity, II_c, kA/m	875 to 1035	716 to 844	1018 to 1123
Intrinsic coercivity, iH_c, kA/m	min. 1114	min. 1989	min. 1114
$(BH)_{max}$, kJ/m^3	278 to 319	183 to 223	342 to 390
Relative recoil magnetic permeability		1.03 to 1.06	
Temperature coefficient α_B of B_r at 20 to 100°C, %/°C		−0.11 to −0.13	
Temperature coefficient α_{iH} of iH_c at 20 to 100°C, %/°C		−0.65 to −0.72	
Curie temperature, °C		≈ 310	
Maximum continuous service temperature, °C	160	180	140
Thermal conductivity, W/(m°C)		≈ 7.7	
Specific mass dens., ρ_{PM}, kg/m^3		7500	
Electric conductivity, $\times 10^6$ S/m		≈ 0.67	
Coefficient of thermal expansion at 20 to 100°C, $\times 10^{-6}$/°C		−1.5	
Young's modulus, $\times 10^6$ MPa		0.150	
Bending stress, MPa		260	
Vicker's hardness		≈ 600	
Features	High energy product	High temperature	Super high performance

is placed inside a closed ideal ferromagnetic circuit, i.e. toroid, this PM does not show any magnetic properties in the external space, in spite of the fact that there is the magnetic flux

$$\Phi_r = B_r S_M = B_r w_M l_M \tag{3.16}$$

corresponding to the remanent flux density B_r inside the PM.

A PM previously magnetized and placed alone in an open space, as in Fig. 3.9a, generates a magnetic field. To sustain a magnetic flux in the external open space, an MMF developed by the magnet is necessary. The state of the PM is characterized by the point *K* on the demagnetization curve (Fig. 3.10). The location of the point *K* is at the intersection of the demagnetization curve with a straight line representing the permeance of the external magnetic circuit (open space):

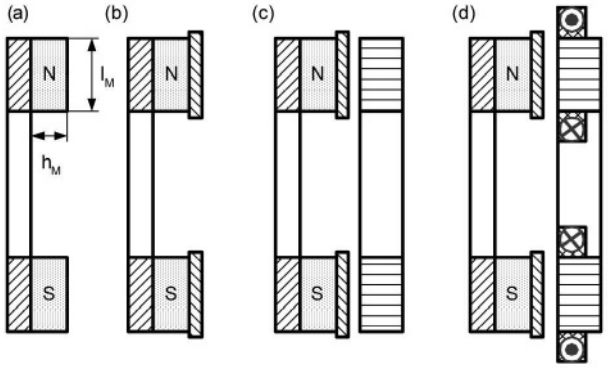

Figure 3.9. Stabilization of a PM: (a) PM alone, (b) PM with pole shoes, (c) PM inside an external magnetic circuit, (d) PM with a complete external armature system.

$$G_{ext} = \frac{\Phi_K}{\mathcal{F}_K}, \qquad \tan\alpha_{ext} = \frac{\Phi_K/\Phi_r}{\mathcal{F}_K/\mathcal{F}_c} = G_{ext}\frac{\mathcal{F}_c}{\Phi_r} \tag{3.17}$$

The permeance G_{ext} corresponds to the flux Φ—MMF coordinate system and is referred to as MMF at the ends of the PM. In the Φ—MMF coordinate system the remanent flux Φ_r is according to eqn (3.16) and the MMF corresponding to the coercivity H_c is

$$\mathcal{F}_c = H_c h_M \tag{3.18}$$

The magnetic energy per unit produced by the PM in the external space is $w_K = B_K H_K/2$. This energy is proportional to the rectangle limited by the coordinate system and lines perpendicular to the Φ and $\mathcal{F}$ coordinates projected from the point *K*. It is obvious that the maximum magnetic energy is for $B_K = B_{max}$ and for $H_K = H_{max}$.

If the poles are furnished with pole shoes (Fig. 3.9b) the permeance of the external space increases. The point which characterizes a new state of the PM in Fig. 3.10 moves along the recoil line from the point *K* to the point *A*. The recoil line KG_M is the same as the internal permeance of the PM, i.e.

$$G_M = \mu_{rec}\frac{w_M l_M}{h_M} = \mu_{rec}\frac{S_M}{h_M} \tag{3.19}$$

The point *A* is the intersection of the recoil line KG_M and the straight line OG_A representing the leakage permeance of the PM with pole shoes, i.e.

$$G_A = \frac{\Phi_A}{\mathcal{F}_A}, \qquad \tan\alpha_A = G_A\frac{\mathcal{F}_c}{\Phi_r} \tag{3.20}$$

The energy produced by the PM in the external space decreases as compared with the previous case, i.e. $w_A = B_A H_A/2$.

The next stage is to place the PM in an external ferromagnetic circuit as shown in Fig. 3.9c. The resultant permeance of this system is

$$G_P = \frac{\Phi_P}{\mathcal{F}_P}, \qquad \tan\alpha_P = G_P \frac{\mathcal{F}_c}{\Phi_r} \tag{3.21}$$

which meets the condition $G_P > G_A > G_{ext}$. For an external magnetic circuit without any electric circuit carrying the armature current, the magnetic state of the PM is characterized by the point *P* (Fig. 3.10), i.e. the intersection of the recoil line KG_M and the permeance line OG_P.

When the external magnetic circuit is furnished with an armature winding and when this winding is fed with a current which produces an MMF magnetizing the PM (Fig. 3.9d), the magnetic flux in the PM increases to the value Φ_N. The d-axis MMF $\mathcal{F}'_{ad}$ of the external (armature) field acting directly on the PM corresponds to Φ_N. The magnetic state of the PM is described by the point *N* located on the recoil line on the right-hand side of the origin of the coordinate system. To obtain this point it is necessary to lay off the distance $O\mathcal{F}'_{ad}$ and to draw a line G_P from the point $\mathcal{F}'_{ad}$ inclined by the angle α_P to the *F*-axis. The intersection of the recoil line and the permeance line *Gp* gives the point *N*. If the exciting current in the external armature winding is increased further, the point *N* will move further along the recoil line to the right, up to the saturation of the PM.

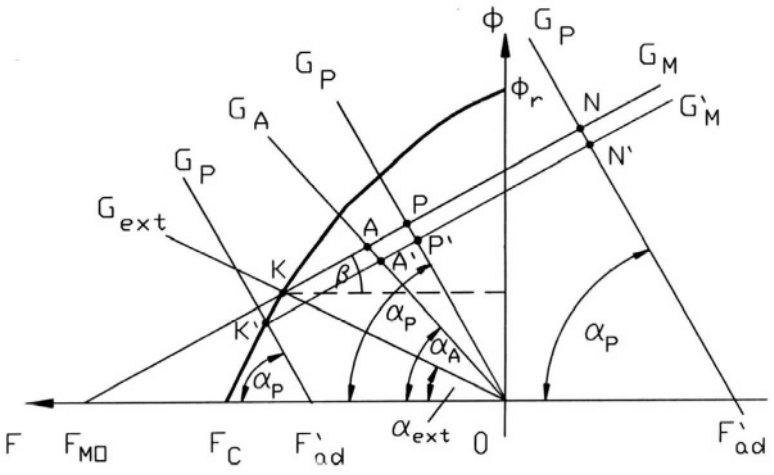

Figure 3.10. Diagram of a PM for finding the origin of the recoil line and operating point.

When the excitation current is reversed, the external armature magnetic field will demagnetize the PM. In this case it is necessary to lay off the distance $O\mathcal{F}'_{ad}$ from the origin of the coordinate system to the left (Fig. 3.10). The line G_P drawn from the point $\mathcal{F}'_{ad}$ with the slope α_P intersects the demagnetization curve at the point K' . This point can be above or below the point *K* (for the PM alone in the open space). The point K' is the origin of a new recoil line $K'G'_M$. Now if the armature exciting current decreases, the operating point will move along the new recoil line $K'G'_M$ to the right. If the armature current drops down to zero, the operating point takes the position P' (intersection of the new recoil line $K'G'_M$ with the permeance line G_P drawn from the origin of the coordinate system).

On the basis of Fig. 3.10 the energies $w_{P'} = B_{P'}H_{P'}/2$, $w_P = B_P H_P/2$, and $w_{P'} < w_P$. The location of the origin of the recoil line, as well as the location of the operating point, determine the level of utilization of the energy produced by the PM. A *PM behaves differently than a d.c. electromagnet*: the energy of a PM is not constant if the permeance and exciting current of the external armature changes.

The location of the origin of the recoil line is determined by the minimum value of the permeance of the external magnetic circuit or the demagnetization action of the external field.

To obtain the properties of PMs more independent of the external magnetic fields, PMs need to be stabilized. *Stabilization* means the PM is demagnetized up to a value which is slightly higher than the most dangerous demagnetization field during the operation of a system where the PM is installed. In magnetic circuits with stabilized PMs the operating point describing the state of the PM is located on the recoil line.

More details about how to find the operating point of a PM graphically and analytically can be found in [96].

3.2.4 Permeances for main and leakage fluxes

Permeances of air gaps and permeances for leakage fluxes can be found analytically by dividing the magnetic field into simple solids. Permeances of simple solids shown in Fig. 3.11 can be found using the following formulae:

(a) Rectangular prism (Fig. 3.11a)

$$G = \mu_0 \frac{w_M l_M}{g} \quad \text{H} \tag{3.22}$$

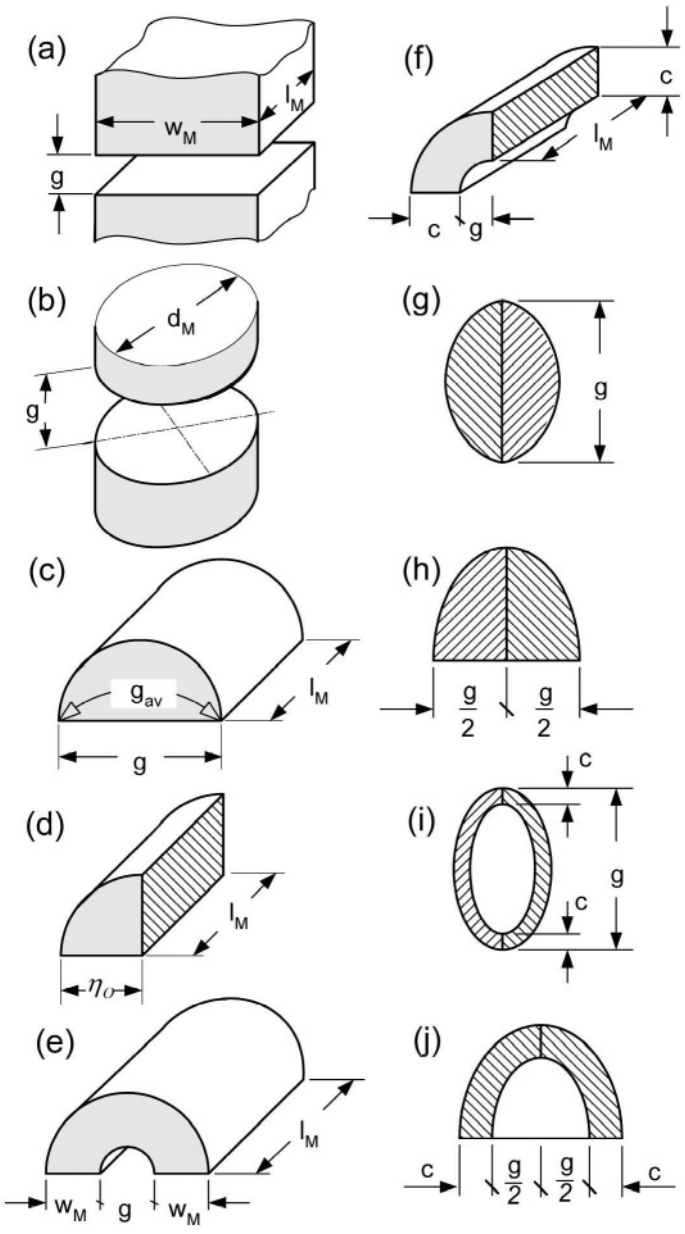

Figure 3.11. Simple solids: (a) rectangular prism, (b) cylinder, (c) half-cylinder, (d) one-quarter of a cylinder, (e) half-ring, (f) one-quarter of a ring, (g) one-quarter of a sphere, (h) one-eighth of a sphere, (i) one-quarter of a shell, (j) one-eighth of a shell.

(b) Cylinder (Fig. 3.11b)

$$G = \mu_0 \frac{\pi d_M^2}{4g} \tag{3.23}$$

(c) Half-cylinder (Fig. 3.11c)

$$G = 0.26 \mu_0 l_M \tag{3.24}$$

where the average air gap $g_{av} = 1.22g$ and the surface $w_M l_M$ should be replaced by $0.322 g l_M$ [13]

(d) One-quarter of a cylinder (Fig. 3.11d)

$$G = 0.52 \mu_0 l_M \tag{3.25}$$

(e) Half-ring (Fig. 3.11e)

$$G = \mu_0 \frac{2 l_M}{\pi (g/w_M + 1)} \tag{3.26}$$

For $g < 3w_M$,

$$G = \mu_0 \frac{l_M}{\pi} \ln \left(1 + \frac{2w_M}{g} \right) \tag{3.27}$$

(f) One-quarter of a ring (Fig. 3.11f)

$$G = \mu_0 \frac{2 l_M}{\pi (g/c + 0.5)} \tag{3.28}$$

For $g < 3c$,

$$G = \mu_0 \frac{2 l_M}{\pi} \ln \left(1 + \frac{c}{g} \right) \tag{3.29}$$

(g) One-quarter of a sphere (Fig. 3.11g)

$$G = 0.077 \mu_0 g \tag{3.30}$$

(h) One-eighth of a sphere (Fig. 3.11h)

$$G = 0.308\mu_0 g \tag{3.31}$$

(i) One-quarter of a shell (Fig. 3.11i)

$$G = \mu_0 \frac{c}{4} \tag{3.32}$$

(j) One-eighth of a shell (Fig. 3.11j)

$$G = \mu_0 \frac{c}{2} \tag{3.33}$$

Fig. 3.12 shows a model of a flat electrical machine with smooth armature core (without slots) and surface PM excitation system. The armature is of steel laminations. The PMs are fixed to the mild steel yoke.

The pole pitch is τ, the width of each PM is w_M, and its length is l_M. In an AFPM machine

$$l_M = 0.5(D_{out} - D_{in}) \tag{3.34}$$

The space between the pole face and the armature core is divided into a prism (1), four quarters of cylinders (2 and 4), four quarters of rings (3 and 5), four pieces of 1/8 of a sphere (6) and four pieces of 1/8 of a shell (7). Formulae for the permeance calculations have been found on the assumption that the permeance of a solid is equal to its average cross section area to the average length of the flux line. If we ignore the fringing flux, the permeance of a rectangular air gap per pole (prism 1 in Fig. 3.12) is

$$G_{g1} = \mu_0 \frac{w_M l_M}{g'} \tag{3.35}$$

The equivalent air gap g' is only equal to the nonmagnetic gap (mechanical clearance) g for a slotless and unsaturated armature. To take into account slots (if they exist) and magnetic saturation, the air gap g is increased to $g' = gk_C k_{sat}$, where $k_C > 1$ is Carter's coefficient taking into account slots (1.2), and $k_{sat} > 1$ is the saturation factor of the magnetic circuit defined as

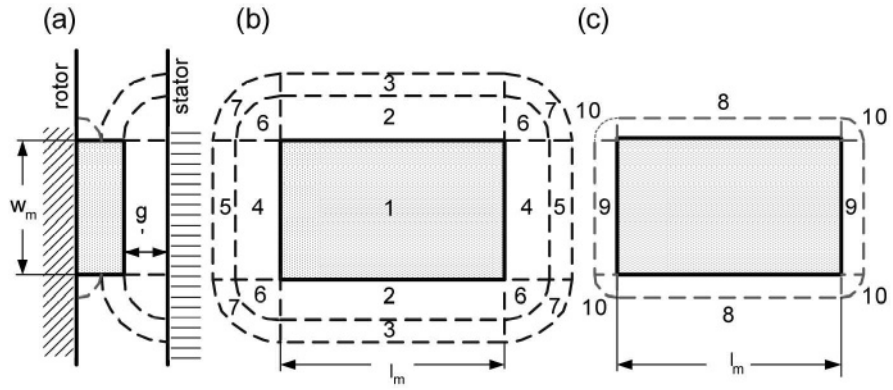

Figure 3.12. Electrical machine with flat slotless armature and flat PM excitation system — division of the space occupied by the magnetic field into simple solids: (a) longitudinal section, (b) air gap field, (c) leakage field (between the PM and steel yoke).

the ratio of the MMF per pole pair to the air gap magnetic voltage drop (MVD) taken twice [96].

To take into account the fringing flux it is necessary to include all paths for the magnetic flux coming from the excitation system through the air gap to the armature system (Fig. 3.12), i.e.

$$G_g = G_{g1} + 2(G_{g2} + G_{g3} + G_{g4} + G_{g5}) + 4(G_{g6} + G_{g7}) \tag{3.36}$$

where G_{g1} is the air gap permeance according to eqn (3.35) and G_{g2} to G_{g7} are the air gap permeances for fringing fluxes. The permeances G_{g2} to G_{g5} can be found using eqns (3.25), (3.28), (3.31) and (3.32).

In a similar way the resultant permeance for the leakage flux of the PM can be found, i.e.

$$G_{lM} = 2(G_{l8} + G_{l9}) + 4G_{l10} \tag{3.37}$$

where G_{l8}, G_{l9} (one-quarter of a cylinder) and G_{l10} (one-eight of a sphere) are the permeances for leakage fluxes between the PM and rotor yoke according to Fig. 3.12c — eqns (3.25) and (3.31).

3.2.5 Calculation of magnetic circuits with PMs

The *equivalent magnetic circuit of a PM system* with armature is shown in Fig. 3.13. The reluctances of pole shoes (mild steel) and armature stack (electrotechnical laminated steel) are much smaller than those of the air gap and

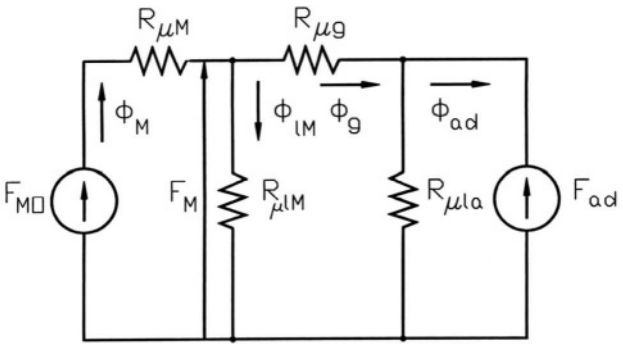

Figure 3.13. Equivalent circuit (in the d-axis) of a PM system with armature.

PM and have been neglected. The "open circuit" MMF acting along the internal magnet permeance $G_M = 1/\Re_{\mu M}$ is $\mathcal{F}_{M0} = H_{M0}h_M$, the d-axis armature reaction MMF is $\mathcal{F}_{ad}$, the total magnetic flux of the PM is Φ_M, the leakage flux of the PM is Φ_{lM}, the useful air gap magnetic flux is Φ_g, the leakage flux of the external armature system is Φ_{la}, the flux in the d-axis produced by the armature is Φ_{ad} (demagnetizing or magnetizing), the reluctance for the PM leakage flux is $\Re_{\mu lM} = 1/G_{lM}$, the air gap reluctance is $\Re_{\mu g} = 1/G_g$, and the external armature leakage reluctance is $\Re_{\mu la} = 1/G_{gla}$. The following Kirchhoff's equations can be written on the basis of the equivalent circuit shown in Fig. 3.13

$$\Phi_M = \Phi_{lM} + \Phi_g$$

$$\Phi_{la} = \frac{\pm\mathcal{F}_{ad}}{\Re_{\mu la}}$$

$$\mathcal{F}_{M0} - \Phi_M\Re_{\mu M} - \Phi_{lM}\Re_{\mu lM} = 0$$

$$\Phi_{lM}\Re_{lM} - \Phi_g\Re_{\mu g} \mp \mathcal{F}_{ad} = 0$$

The solution to the above equation system yields the air gap magnetic flux:

$$\Phi_g = \left[\mathcal{F}_{Mo} \mp \mathcal{F}_{ad}\frac{G_g}{G_g + G_{lM}}\frac{(G_g + G_{lM})(G_M + G_{lM})}{G_gG_M}\right]\frac{G_gG_M}{G_g + G_{lM} + G_M}$$

or

$$\Phi_g = \left[\mathcal{F}_{M0} \mp \mathcal{F}'_{ad}\frac{G_t(G_M + G_{lM})}{G_gG_M}\right]\frac{G_gG_M}{G_t + G_M} \tag{3.38}$$

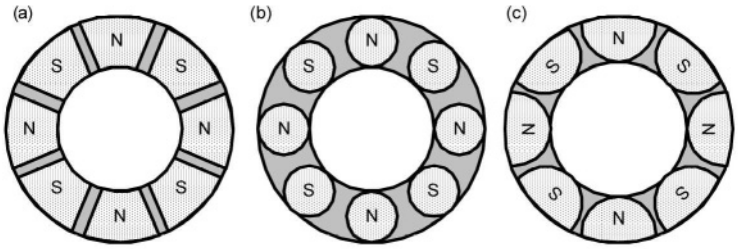

Figure 3.14. Shapes of PM rotors of disc-type machines: (a) trapezoidal, (b) circular, (c) semicircular.

where the total resultant permeance G_t for the flux of the PM is

$$G_t = G_g + G_{lM} = \sigma_{lM} G_g \tag{3.39}$$

and the direct-axis armature MMF acting directly on the PM is

$$\mathcal{F}'_{ad} = \mathcal{F}_{ad} \frac{G_g}{G_g + G_{lM}} = \mathcal{F}_{ad} \left(1 + \frac{G_{lM}}{G_g}\right)^{-1} = \frac{\mathcal{F}_{ad}}{\sigma_{lM}} \tag{3.40}$$

The upper sign in eqn (3.38) is for the demagnetizing armature flux and the lower sign is for the magnetizing armature flux.

The coefficient of the PM leakage flux (3.9) can also be expressed in terms of permeances, i.e.

$$\sigma_{lM} = 1 + \frac{\Phi_{lM}}{\Phi_g} = 1 + \frac{G_{lM}}{G_g} \tag{3.41}$$

3.2.6 Fabrication of rotor magnetic circuits

Magnetic circuits of rotors of AFPM brushless machines provide the excitation flux and are designed as:

- PMs glued to a ferromagnetic ring or disc which serves as a backing magnetic circuit (yoke);
- PMs arranged into Halbach array without any ferromagnetic core.

Shapes of PMs are usually trapezoidal, circular or semicircular (Fig. 3.14). The shape of PMs affects the distribution of the air gap magnetic field and contents of higher space harmonics. The output voltage quality (harmonics of

Table 3.13. Magnetization curves of solid ferromagnetic materials: 1 — carbon steel (0.27%C), 2 — cast iron

Magnetic flux density, B	Magnetic field intensity, H	
	Mild carbon steel 0.27% C	Cast iron
T	A/m	A/m
0.2	190	900
0.4	280	1600
0.6	320	3000
0.8	450	5150
1.0	900	9500
1.2	1500	18,000
1.4	3000	28,000
1.5	1500	
1.6	6600	
1.7	11,000	

the EMF) of AFPM generators depends on the PM geometry (circular, semi-circular, trapezoidal) and distance between adjacent magnets [75].

Since the magnetic flux in the rotor magnetic circuit is stationary, mild steel (carbon steel) backing rings can be used. Rings can be cut from 4 to 6 mm mild steel sheets. Table 3.13 shows magnetization characteristics B–H of a mild carbon steel and cast iron. Electrical conductivities of carbon steels are from 4.5×10^6 to 7.0×10^6 S/m at 20°C.

Halbach array

Twin rotors of double-sided coreless AFPM machines (Fig. 1.4d) may use PMs arranged in *Halbach array* [104–106]. The key concept of Halbach array is that the magnetization vector of PMs should rotate as a function of distance

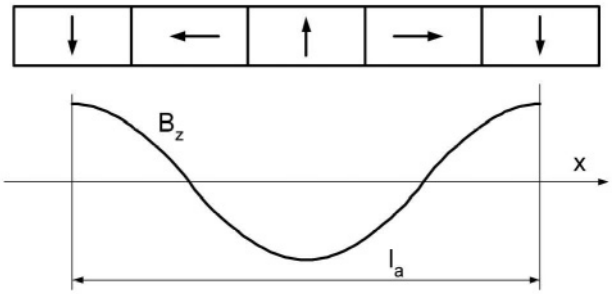

Figure 3.15. Cartesian Halbach array.

along the array (Fig. 3.15) [104–106]. Halbach array has the following advantages:

- the fundamental field is stronger by a factor of 1.4 than in a conventional PM array, and thus the power efficiency of the machine is doubled;
- the array of PMs does not require any backing steel magnetic circuit and PMs can be bonded directly to a non-ferromagnetic supporting structure (aluminum, plastics);
- the magnetic field is more sinusoidal than that of a conventional PM array;
- Halbach array has very low back-side fields.

The peak value of the magnetic flux density at the active surface of Halbach array is

$$B_{m0} = B_r[1 - \exp(-\beta h_M)]\frac{\sin(\pi/n_M)}{\pi/n_M} \tag{3.42}$$

where B_r is the remanent magnetic flux density of the magnet, $\beta = 2\pi/l_a$ - see also eqn (1.6), l_a is the spatial period (wavelength) of the array and n_M is the number of PM pieces per wavelength. For the array shown in Fig. 3.15 $n_M = 4$. For example, assuming $B_r = 1.25$ T, $h_M = 6$ mm, $l_a = 24$ mm, $n_m = 4$ (rectangular PMs), the peak magnetic flux density at the surface of Halbach array $B_{M0} = 0.891$ T.

The tangential B_x and normal B_z components of Halbach array at the distance z from the surface of PMs are

$$B_x(x,z) = B_{m0}cos(\beta x)exp(-\beta z) \tag{3.43}$$

$$B_z(x,z) = B_{m0}sin(\beta x)exp(-\beta z) \tag{3.44}$$

For a double-sided configuration of Halbach arrays, i.e. twin disc external rotors, the tangential and normal component of the magnetic flux density distribution in the space between discs are

$$B_x(x,z) = B_{m0}\frac{1}{\beta}\cos(\beta x)\frac{1}{\cosh(\beta t/2)}\sinh(\beta z) \tag{3.45}$$

$$B_z(x,z) = B_{m0}sin(\beta x)\frac{1}{\cosh(\beta t/2)}\cosh(\beta z) \tag{3.46}$$

where B_{m0} is according to eqn (3.42) and t is magnet–to–magnet distance between two halves of the disc. The origin of the $0xyz$ coordinate system is as in Fig. 1.8.

3.3 Windings

3.3.1 Conductors

Stator (armature) windings of electric motors are made of solid *copper conductor wires* with round or rectangular cross sections.

The *electric conductivity* at 20°C of copper wires is $57 \times 10^6 \geq \sigma_{20} \geq 56 \times 10^6$ S/m. For aluminum wires $\sigma_{20} \approx 33 \times 10^6$ S/m. The electric conductivity is temperature dependent and for $\theta - 20^{\circ} \leq 150^{\circ}$C can be expressed as

$$\sigma = \frac{\sigma_{20}}{1 + \alpha(\theta - 20^{\circ})} \tag{3.47}$$

where α is the *temperature coefficient of electric resistance*. For copper wires $\alpha = 0.00393$ 1/°C and for aluminum wires $\alpha = 0.00403$ 1/°C. For $\vartheta - 20^{\circ} > 150^{\circ}$C eqn (3.47) contains two temperature coefficients α and β of the electric resistance, i.e.

$$\sigma = \frac{\sigma_{20}}{1 + \alpha(\vartheta - 20^{\circ}) + \beta(\vartheta - 20^{\circ})^2} \tag{3.48}$$

The *maximum temperature rise* for the windings of electrical machines is determined by the temperature limits of insulating materials. The maximum temperature rise in Table 3.14 assumes that the temperature of the cooling medium $\vartheta_c \leq 40^{\circ}$C. The maximum temperature of windings is actually

$$\vartheta_{max} = \vartheta_c + \Delta\vartheta \tag{3.49}$$

where $\Delta\vartheta$ is the maximum allowable temperature rise according to Table 3.14. A polyester-imide and polyamide-imide coat can provide an operating temperature of 200°C. The highest operating temperatures (over 600°C) can be achieved using *nickel clad copper* or *palladium-silver* conductor wires and ceramic insulation.

3.3.2 Fabrication of slotted windings

Stator windings are usually made of insulated copper conductors. The cross section of conductors can be circular or rectangular. For large AFPM machines a direct water cooling system and consequently hollow conductors can be considered.

It is difficult to make and form stator coils if the round conductor is thicker than 1.5 mm. If the current density is too high, parallel conductor wires of

Table 3.14. Maximum temperature rise $\Delta\vartheta$ for armature windings of electrical machines according to IEC and NEMA (based on 40°C ambient temperature)

Rated power of machines, length of core and voltage	Insulation class A °C	E °C	B °C	F °C	H °C
IEC a.c. machines < 5000 kVA (resistance method)	60	75	80	100	125
IEC a.c. machines ≥ 5000 kVA or length of core ≥ 1 m (embedded detector method)	60	70	80	100	125
NEMA a.c. machines ≤ 1500 hp (embedded detector method)	70	–	90	115	140
NEMA a.c. machines > 1500 hp and ≤ 7 kV (embedded detector method)	65	–	85	110	135

smaller diameter are recommended rather than one thicker wire. Stator windings can also have parallel current paths.

The armature windings can be either *single-layer* or *double layer* (Section 2.2). After coils are wound, they must be secured in place, somehow, so as to avoid conductor movement. Two standard methods are used to secure the conductors of electrical machines in place:

- *dipping* the whole component into a varnish-like material, and then baking off its solvent,
- *trickle impregnation* method, which uses heat to cure a catalyzed resin which is dripped onto the component.

Polyester, epoxy or silicon resins are used most often as impregnating materials for treatment of stator windings. Silicon resins of high thermal endurance are able to withstand $\vartheta_{max} > 225°C$.

Recently, a new method of conductor securing that does not require any additional material, and uses very low energy input, has emerged [163]. The solid conductor wire (usually copper) is coated with a *heat and/or solvent activated adhesive.* The adhesive which is usually a polyvinyl butyral, utilizes a low temperature thermoplastic resin [163]. This means that the bonded adhesive can come apart after a certain minimum temperature is reached, or it again comes in contact with the solvent. Normally this temperature is much lower than the

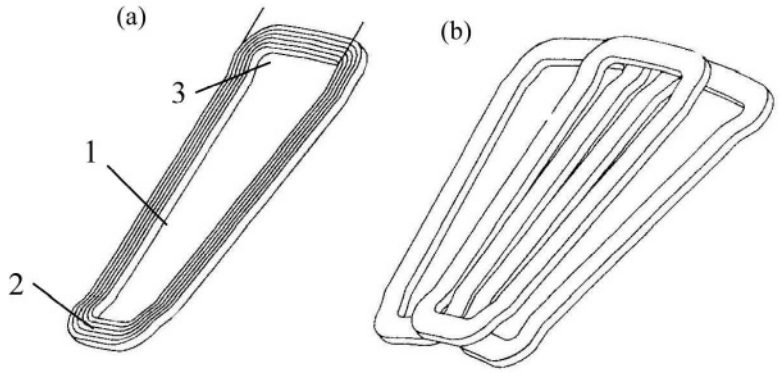

Figure 3.16. Disc-type coreless winding assembled of coils of the same shape according to U.S. Patent No. 5 744 896 [139]: (a) single coil; (b) three adjacent coils. 1 — coil side, 2 — inner offsetting bend, 3 — outer offsetting bend.

thermal rating of the base insulation layer. The adhesive is activated by either passing the wire through a solvent while winding or heating the finished coil as a result of passing electric current through it.

The conductor wire with a heat activated adhesive overcoat costs more than the same class of non-bondable conductor. However, a less than two second current pulse is required to bond the heat activated adhesive layer and bonding machinery costs about half as much as trickle impregnation machinery [163].

3.3.3 Fabrication of coreless windings

Stator coreless windings of AFPM machines are fabricated as uniformly distributed coils on a disc-type cylindrical supporting structure (hub) made of nonmagnetic and nonconductive material. There are two types of windings:

(a) winding comprised of multi-turn coils wound with turns of insulated conductor of round or rectangular cross section;

(b) printed winding also called *film coil winding.*

Coils are connected in groups to form the phase windings typically connected in star or delta. Coils or groups of coils of the same phase can be connected in parallel to form parallel paths.

To assemble the winding of the same coils and obtain high density packing, coils should be formed with *offsetting bends,* as shown in Fig. 3.16. The space between two sides of the same coil is filled with coil sides from each of the adjacent coils.

Coils can be placed in a slotted structure of the mould (Fig. 3.17). With all the coils in position, the winding (often with a supporting structure or hub) is

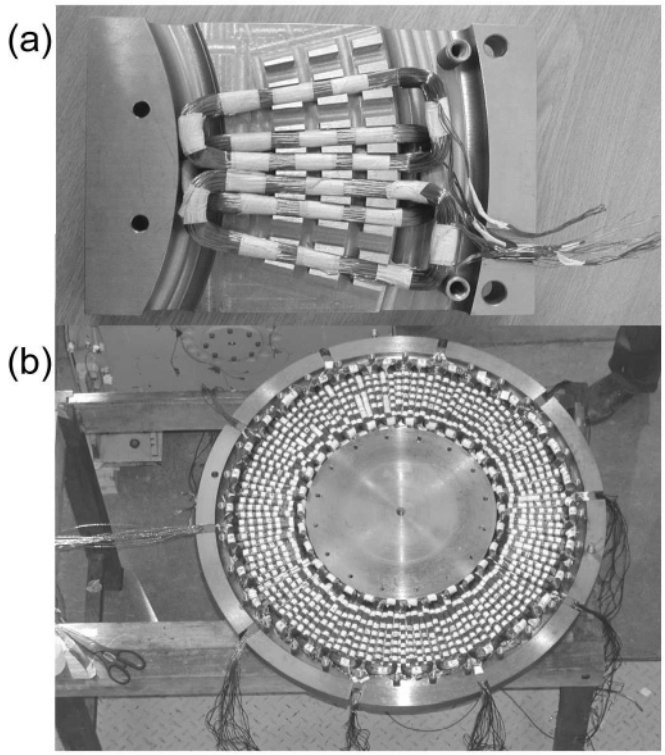

Figure 3.17. Moulds for positioning the coils: (a) mould with guide slots; (b) mould with guide pins.

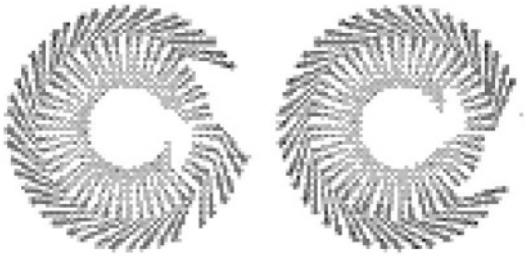

Figure 3.18. Film coils for AFPM micromotors. Courtesy of *EMbest,* Soeul, Korea.

moulded into a mixture of epoxy resin and hardener and then cured in a heated oven. Because of the difficulty of releasing the cured stator from the slotted structure of the mould (Fig. 3.17a), each spacing block that forms a guide slot consists of several removable pins of different size (Fig. 3.17b).

For very small AFPM machines and micromachines printed circuit coreless windings allow for automation of production. Printed circuit windings for

AFPM brushless machines fabricated in a similar way as printed circuit boards have not been commercialized due to poor performance. A better performance has been achieved using film coil windings made through the same process as flexible printed circuits [85]. The coil pattern is formed by etching two copper films that are then attached to both sides of a board made of insulating materials (Fig. 3.18). Compact coil patterns are made possible by connecting both sides of coil patterns through holes [85].

Numerical example 3.1

A simple stationary magnetic circuit is shown in Fig. 3.19. There are two Vacomax 240 HR SmCo PMs (Table 3.11) with $B_r = 1.10$ T, $H_c = 680$ kA/m, temperature coefficients $\alpha_B = -0.03\%/^{\circ}\text{C}$ and $\alpha_H = -0.15\%/^{\circ}\text{C}$ at $20 \leq \vartheta_{PM} \leq 100^{\circ}\text{C}$. The height of the PM per pole is $h_M = 6$ mm and the air gap thickness $g = 1$ mm. The U-shaped and I-shaped (top) ferromagnetic cores are made of a laminated electrotechnical steel. The width of the magnets and cores is 17 mm. Calculate the air gap magnetic flux density, air gap magnetic field strength, the useful energy of PMs and normal attractive force per two poles at: (a) $\vartheta_{PM} = 20^{\circ}\text{C}$ and (b) $\vartheta_{PM} = 100^{\circ}\text{C}$. The MVD in the laminated core, leakage and fringing magnetic flux can be neglected.

Solution:

(a) Magnet temperature $\vartheta_{PM} = 20^{\circ}\text{C}$

The relative recoil magnetic permeability according to eqn (3.4) for a straight linc demagnetization curve is

$$\mu_{rrcc} = \frac{1}{\mu_0}\frac{\Delta B}{\Delta H} = \frac{1}{0.4\pi \times 10^{-6}}\frac{1.10 - 0}{680,000 - 0} \approx 1.29$$

The air gap magnetic flux density according to eqn (3.13) is

$$B_g \approx \frac{1.10}{1 + 1.29 \times 1.0/6.0} = 0.906 \text{ T}$$

The air gap magnetic field strength according to eqn (3.14) in which $H = H_g$ and $B = B_g$ is

$$H_g = H_c\left(1 - \frac{B_g}{B_r}\right) = 680 \times 10^3\left(1 - \frac{1.064}{1.10}\right) = 120.12 \times 10^3 \text{ A/m}$$

The useful energy per magnet volume according to eqn (3.5) is

$$w_g = \frac{B_g H_g}{2} = \frac{1.064 \times 120,120}{2} = 54\,395.8 \text{ J/m}^3$$